Available online at www.sciencedirect.com
SCIENCE DIRECT®
Journal of Solid State Chemistry 177 (2004) 4557–4563
JOURNAL OF SOLID STATE CHEMISTRY
www.elsevier.com/locate/jssc

Copper phosphonates with dinuclear and layer structures: a structural and magnetic study

Hong-Chang Yao[a], Yi-Zhi Li[a], Song Gao[b], You Song[a], Li-Min Zheng[a,*], Xin-Quan Xin[a]

[a]*State Key Laboratory of Coordination Chemistry, Department of Chemistry, Coordination Chemistry Institute, Nanjing University, Nanjing City, Jiangsu Province 210093, PR China*

[b]*State Key Lab of Rare Earth Materials Chemistry and Applications, College of Chemistry and Molecular Engineering, Peking University, Beijing 100870, PR China*

Received 16 August 2004; received in revised form 6 September 2004; accepted 10 September 2004
Available online 11 November 2004

Abstract

Hydrothermal reactions of copper (II) nitrate with 1-hydroxycyclohexanephosphonic acid $[C_6H_{10}(OH)PO_3H_2]$ or Δ^1-cyclohexenephosphonic acid $[C_6H_9PO_3H_2]$ have resulted in three new copper phosphonates, namely, $Cu(C_6H_{10}(OH)PO_3)(H_2O)_2$ (**1**), $Cu(C_6H_{10}(OH)PO_3)$ (**2**) and $Cu(C_6H_9PO_3)(H_2O)$ (**3**). Compound **1** has a dinuclear structure in which two $\{CuO_5\}$ square pyramids are bridged by two $\{CPO_3\}$ tetrahedra through corner sharing. The dimers are connected through intermolecular hydrogen bonds, forming supramolecular layers. Both compounds **2** and **3** show layer structures typical for metal mono-phosphonates, in which the inorganic metal-containing layers are separated by cyclohexane or cyclohexene groups. The magnetic studies show that ferromagnetic interactions are mediated between copper centers in compound **1**. In compounds **2** and **3**, antiferromagnetic interactions are dominant.

Keywords: Copper; Phosphonates; Structures; 1-hydroxycyclohexanephosphonic; Δ^1-cyclohexenephosphonic; Magnetic properties

1. Introduction

A variety of metal organo-phosphonate compounds have been prepared in the past decades primarily due to their potential applications in catalysis, ion exchange and absorption, proton conductivity, sensors and material chemistry [1–5]. One remarkable feature of these compounds is that they are capable of combining the properties of the organic pendant groups along with those of the inorganic host, and hence their electronic, optical and magnetic properties can be modulated within the layers.

Although other types of structures are known, many phosphonates exhibit layered or pillared layered character, in which the inorganic metal-containing layers are separated by organic groups, thus offering the possibility of magnetic studies in confined 2D systems [6–9]. In the literature, magnetic studies have been performed on compounds $M^{II}(RPO_3)(H_2O)$ or $M^{II}_2(O_3PRPO_3)(H_2O)_2$ with layered or pillared layered structures as well as compounds with other types of structures. Interesting weak ferromagnetism and metamagnetism have been observed [10,11].

In this paper, we report three new copper phosphonates, $Cu(C_6H_{10}(OH)PO_3)(H_2O)_2$ (**1**), $Cu(C_6H_{10}(OH)PO_3)$ (**2**) and $Cu(C_6H_9PO_3)(H_2O)$ (**3**) by using 1-hydroxycyclohexanephosphonic $[C_6H_{10}(OH)PO_3H_2]$ and Δ^1-cyclohexenephosphonic $[C_6H_9PO_3H_2]$ acids. Although compounds **2** and **3** show layer structures typical for metal mono-phosphonates, a discrete dinuclear structure is found in compound **1**. Their magnetic properties are investigated.

*Corresponding author. Fax: +86 25 8331 4502.
E-mail address: lmzheng@netra.nju.edu.cn (L.-M. Zheng).

0022-4596/$ - see front matter © 2004 Elsevier Inc. All rights reserved.
doi:10.1016/j.jssc.2004.09.007

2. Experimental

2.1. Materials and methods

1-Hydroxycyclohexanephosphonic acid, $C_6H_{10}(OH)PO_3H_2$, and Δ^1-cyclohexenephosphonic acid, $C_6H_9PO_3H_2$, were prepared according to the literature [12]. Other starting materials were reagent grade and used as purchased. The elemental analyses were performed in a PE 240C elemental analyzer. IR spectra were recorded on a VECTOR 22 spectrometer in the spectral range 4000–400 cm^{-1} using the KBr disk method. Thermal analyses were performed in nitrogen with a heating rate of 10 °C/min on a TGA-DTA V1.1B TA Inst 2100 instrument. Variable-temperature magnetic susceptibility data were obtained on polycrystalline samples (30.2 mg for **1**, 88.17 mg for **2** and 30.2 mg for **3**) from 2 to ca. 300 K in a magnetic field of 20, 2 and 10 kOe, respectively, using a MagLab System 2000 magnetometer (for **1** and **3**) or a Quantum Design SQUID magnetometer (for **2**). Diamagnetic corrections were obtained from Pascal's constants [13].

2.2. Synthesis of $Cu(C_6H_{10}(OH)PO_3)(H_2O)_2$ (1)

A mixture of $Cu(NO_3)_2 \cdot 3H_2O$ (0.5 mmol, 0.1210 g), NaF (0.75 mmol, 0.0315 g), $C_6H_{10}(OH)PO_3H_2$ (0.5 mmol, 0.090 g) and H_2O (10 cm^3) was stirred until clear (pH = 3.4), and transferred to a 25 mL Teflon-lined autoclave. The reaction was carried out at 140 °C for 48 h under auto-generated pressure. After slow cooling to room temperature, light-blue column-like crystals of compound **1** were obtained as a major phase, together with a small amount of plate-like crystals of compound **2**. The crystals of compound **1** were manually collected and were further used for both structural and property measurements. Its purity was judged by powder XRD measurement. Yield: 45% based on Cu. Found: C, 25.93; H, 5.40%. Calcd.: C, 25.97; H, 5.58%. IR (KBr, cm^{-1}): 3374 s, 3180 s (br), 3036 s, 2932 s, 2861 m, 2345 w, 1691 w, 1453 w, 1389 w, 1320 w, 1280 w, 1254 w, 1154 w, 1112 s, 1016 s, 972 s, 939 m, 905 w, 828 w, 703 m, 599 m, 543 w, 490 w, 440 w. Thermogravimetric analysis of compound **1** shows a two-step weight loss in the temperature range 50–200 °C. The total weight loss (20.5%) is slightly higher than the calculated value of 19.5% for the removal of two coordinated water molecules.

2.3. Synthesis of $Cu(C_6H_{10}(OH)PO_3)$ (2)

A mixture of $Cu(NO_3)_2 \cdot 3H_2O$ (0.25 mmol, 0.0605 g), NaF (0.75 mmol, 0.0315 g), $C_6H_{10}(OH)PO_3H_2$ (0.5 mmol, 0.090 g) and H_2O (8 cm^3) was stirred until a clear solution was formed (pH = 3.3). The solution was transferred to a 25 mL Teflon-lined autoclave and heated at 140 °C for 48 h under auto-generated pressure. After slow cooling to room temperature, blue lamellar crystals of compound **2** were obtained as a single phase. Yield: 66.6% based on Cu. Found: C, 29.72; H, 4.42%. Calcd.: C, 29.80; H, 4.55%. IR (KBr, cm^{-1}): 3134 s, 2938 s, 2856 m, 1636 w, 1442 m, 1396 m, 1361 w, 1320 w, 1272 w, 1253 w, 1184 m, 1114 s, 1016 s, 1022 s, 981 s, 937 m, 901 w, 838 w, 807 w, 776 w, 695 m, 627 m, 572 m, 533 w, 509 w, 493 m, 429 w, 412 w.

2.4. Synthesis of $Cu(C_6H_9PO_3)(H_2O)$ (3)

Hydrothermal treatment of a mixture of $Cu(NO_3)_2 \cdot 3H_2O$ (0.2 mmol, 0.0483 g), NaF (0.5 mmol, 0.021 g), $C_6H_9PO_3H_2$ (0.2 mmol, 0.0324 g) and H_2O (8 cm^3) at 140 °C for 48 h resulted in blue lamellar crystals as a single phase. Found: C, 29.59; H, 4.66%. Calcd.: C, 29.80; H, 4.55%. IR (KBr, cm^{-1}): 3277 s, 3034 s, 2928 s, 2856 m, 1633 m, 1570 m, 1433 m, 1333 w, 1268 w, 1241 m, 1069 s, 1023 s, 996 s, 932 m, 912 m, 872 m, 799 w, 734 w, 614 m, 587 m, 559 m, 527 m, 407 m. The strong band at 1633 cm^{-1} is due to the C=C group of the cyclohexene ring. The thermogravimetric analysis of compound **3** shows one-step decomposition below 200 °C. The observed weight loss (calcd. 7.94%) corresponds to the release of one water molecule (calc. 7.45%).

Fluoride was added in order to improve the crystallization of the final products. The title compounds (**1, 2** and **3**) can also be obtained without it.

2.5. Crystallographic studies

Single crystals of dimensions $0.2 \times 0.15 \times 0.15\,mm^3$ for **1**, $0.15 \times 0.1 \times 0.08\,mm^3$ for **2** and $0.2 \times 0.1 \times 0.03\,mm^3$ for **3** were used for structure determination. The data were collected on a Bruker SMART APEX CCD diffractometer using graphite-monochromatized Mo$K\alpha$ radiation ($\lambda = 0.71073$ Å) at room temperature. The data were integrated using a Siemens SAINT program [14], with the intensities corrected for Lorentz factor, polarization, air absorption, and absorption due to variation in the path length through the detector faceplate. Numbers of measured, unique, and observed reflections [$I > 2\sigma(I)$] are 3088, 2269 and 1779 ($R_{int} = 0.0329$) for **1**, 3759, 1631, 1283 ($R_{int} = 0.054$) for **2** and 4769, 1920 and 1373 ($R_{int} = 0.0459$) for **3**. Empirical absorptions were applied for all compounds.

The structures were solved by direct methods and refined on F^2 by full-matrix least squares using SHELXTL [15]. All the nonhydrogen atoms were refined anisotropically. The hydrogen atoms of the cyclohexyl and cyclohexenyl were placed in calculated positions (C–H = 0.96 Å) and allowed to ride on their respective parent atoms. The H atoms in the H_2O and

hydroxy group were found from the Fourier difference maps and refined isotropically.

3. Results and discussion

3.1. Description of crystal structures

The structures of $Cu(C_6H_{10}(OH)PO_3)(H_2O)_2$ (**1**), $Cu(C_6H_{10}(OH)PO_3)$ (**2**) and $Cu(C_6H_9PO_3)(H_2O)$ (**3**) were determined by single crystal X-ray crystallography. Crystallographic and refinement details are listed in Table 1, with selected bond lengths and angles in Tables 2–4 for compounds **1**–**3**, respectively.

The structure of compound **1** consists of discrete dinuclear units of $Cu_2(C_6H_{10}(OH)PO_3)_2(H_2O)_4$, shown in Fig. 1. The overall structure may be described in terms of two copper(II) square pyramids and two phosphonate tetrahedra in a corner-sharing arrangement. The basal plane of each $\{CuO_5\}$ is occupied by one hydroxyl oxygen [O(4A)], two phosphonate oxygen donors [O(1), O(2A)] and one H_2O molecule [O(2W)]. The Cu–O bond distances are in the range 1.949(2)–2.024(2) Å, similar to those in other copper phosphonates [16–19]. The apical position is filled with a second water molecule [O(1W)] with Cu(1)–O(1W) distance 2.137(2) Å. Each $\{CPO_3\}$ tetrahedron of the phosphonate ligand is corner-shared with two equivalent $\{CuO_5\}$ square pyramids through phosphonate oxygens O(1) and O(2), forming an eight-member ring. The remaining phosphonate oxygen [O(3)] is pendant and is involved in the hydrogen bond networks. An inversion center sits in the middle of the eight-member ring. The Cu(1)…Cu(1A) distance within the dimer is 3.704 Å.

Extensive inter-molecular hydrogen bonds are found between the three phosphonate oxygens and water molecules or hydroxyl groups, forming a supramolecular layer in the *ab* plane (Fig. 2). The O…O distances range from 2.616(3) Å for O(4)…O(3^{i}) to 2.785(3) Å for O(1W)…O(1^{ii}) (symmetry codes: i, $x-1$, y, z; ii, $-x$, $-y+1$, $-z+1$). The layers are then held together by van der Waals attractions along the *c*-axis (Fig. 3).

Compound **2** adopts a layer structure. The building unit is shown in Fig. 4 with an atomic labeling scheme. Each Cu atom has a distorted square pyramidal geometry. The four basal sites are occupied by oxygen atoms from three equivalent phosphonate groups [O(1), O(2B), O(3A)] and hydroxy group [O(4B)]. The Cu–O bond lengths are in the range 1.908(4)–2.107(4) Å. The apical position is occupied by O(3C) from another equivalent phosphonate group [Cu(1)–O(3C): 2.288(4) Å]. Each $\{CPO_3\}$ tetrahedron is vertex-shared with four $\{CuO_5\}$ pyramids through three phosphonate oxygens. Consequently, one of the three phosphonate oxygens [O(3)] serves as a μ_3-bridge linking two equivalent Cu atoms. The Cu(1)…Cu(1) distance over the μ_3-O(3) bridge is 3.229 Å. The Cu(1)–O(3)–Cu(1) bond angle is 99.9°. A two-dimensional structure is thus built up in the *ab* plane which contains four and eight-member rings (Fig. 5). The layers are packed together

Table 1
Crystallographic data for **1**, **2** and **3**

Compound	**1**	**2**	**3**
Formula	$C_6H_{15}CuO_6P$	$C_6H_{11}CuO_4P$	$C_6H_{11}CuO_4P$
M	277.69	241.66	241.66
Crystal system	Triclinic	Triclinic	Monoclinic
Space group	$P\bar{1}$	$P\bar{1}$	$P2_1/c$
a (Å)	5.7666(13)	5.835(5)	14.415(3)
b (Å)	6.8336(15)	5.977(5)	7.6125(14)
c (Å)	14.026(3)	12.413(10)	7.5294(13)
α (deg)	101.298(4)	83.685(14)	
β (deg)	94.750(4)	78.448(14)	92.118(4)
γ (deg)	106.017(4)	77.818(12)	
V (Å^3)	515.4(2)	413.6(6)	825.7(3)
Z	2	2	4
D (g cm^{-3})	1.789	1.941	1.944
F (000)	286	246	492
μ(Mo$K\alpha$) (cm^{-1})	22.75	28.03	28.08
R_1, wR_2 [$I>2\sigma(I)$][a]	0.0361, 0.0730	0.0608, 0.1120	0.0418, 0.0814
R_1, wR_2 (all data)[a]	0.0468, 0.0752	0.0766, 0.1158	0.0601, 0.0853
$(\Delta\rho)_{max}$, $(\Delta\rho)_{min}$ (e Å^{-3})	0.554, −0.376	0.430, −0.874	1.304, −0.515

[a] $R_1=\Sigma||F_o|-|F_c||/\Sigma|F_o|$, w$R_2=[\Sigma w(F_o^2-F_c^2)^2/\Sigma w(F_o^2)^2]^{1/2}$.

Table 2
Selected bond lengths (Å) and angles (deg) for **1**

Cu(1)–O(2W)	1.949(2)	O(2W)–Cu(1)–O(1)	92.23(9)
Cu(1)–O(2A)	1.960(2)	O(2A)–Cu(1)–O(1)	93.98(9)
Cu(1)–O(4A)	2.010(2)	O(4A)–Cu(1)–O(1)	156.85(9)
Cu(1)–O(1)	2.024(2)	O(2W)–Cu(1)–O(1W)	87.96(9)
Cu(1)–O(1W)	2.137(2)	O(2A)–Cu(1)–O(1W)	94.97(9)
P(1)–O(1)	1.542(2)	O(2W)–Cu(1)–O(2A)	172.85(9)
P(1)–O(2)	1.549(2)	O(2W)–Cu(1)–O(4A)	86.11(10)
P(1)–O(3)	1.503(2)	O(4A)–Cu(1)–O(1W)	107.68(10)
O(2A)–Cu(1)–O(4A)	86.79(9)	P(1)–O(2)–Cu(1A)	113.71(11)
O(1)–Cu(1)–O(1W)	95.32(9)	C(1)–O(4)–Cu(1A)	116.19(18)

Symmetry transformations: (A) $-x,-y,-z+1$.

Table 3
Selected bond lengths (Å) and angles (deg) for **2**

Cu(1)–O(1)	1.908(4)	O(3A)–Cu(1)–O(4B)	85.91(16)
Cu(1)–O(3A)	1.919(4)	O(2B)–Cu(1)–O(4B)	80.96(16)
Cu(1)–O(2B)	1.945(4)	O(1)–Cu(1)–O(3C)	112.17(16)
Cu(1)–O(4B)	2.107(4)	O(3A)–Cu(1)–O(3C)	80.12(18)
Cu(1)–O(3C)	2.288(4)	O(2B)–Cu(1)–O(3C)	98.95(16)
P(1)–O(1)	1.488(4)	O(4B)–Cu(1)–O(3C)	87.90(15)
P(1)–O(2)	1.487(4)	P(1)–O(1)–Cu(1)	121.1(2)
P(1)–O(3)	1.594(4)	P(1)–O(2)–Cu(1B)	120.8(2)
O(1)–Cu(1)–O(3A)	97.13(17)	P(1)–O(3)–Cu(1A)	125.8(2)
O(1)–Cu(1)–O(2B)	95.34(17)	P(1)–O(3)–Cu(1D)	120.3(2)
O(3A)–Cu(1)–O(2B)	166.87(16)	Cu(1A)–O(3)–Cu(1D)	99.88(18)
O(1)–Cu(1)–O(4B)	159.93(15)	C(1)–O(4)–Cu(1B)	112.3(3)

Symmetry transformations: (A): $-x,-y+1,-z+2$; (B): $-x+1,-y+1,-z+2$; (C): x, $y+1$, z; (D): x, $y-1$, z.

Table 4
Selected bond lengths (Å) and angles (deg) for **3**

Cu(1)–O(1)	1.912(2)	O(1W)–Cu(1)–O(3C)	80.52(10)
Cu(1)–O(2B)	1.967(3)	P(1)–O(2)–Cu(1B)	131.20(16)
Cu(1)–O(3C)	2.372(2)	P(1)–O(3)–Cu(1E)	148.37(14)
Cu(1)–O(3A)	1.964(2)	O(1)–Cu(1)–O(3A)	164.12(10)
Cu(1)–O(1W)	2.008(3)	O(3A)–Cu(1)–O(2B)	90.47(10)
P(1)–O(1)	1.527(3)	O(3A)–Cu(1)–O(1W)	87.69(10)
P(1)–O(2)	1.539(3)	O(1)–Cu(1)–O(3C)	107.03(10)
P(1)–O(3)	1.532(2)	O(2B)–Cu(1)–O(3C)	88.73(9)
O(1)–Cu(1)–O(2B)	93.92(10)	P(1)–O(1)–Cu(1)	126.01(15)
O(1)–Cu(1)–O(1W)	90.73(11)	P(1)–O(3)–Cu(1D)	119.79(14)
O(2B)–Cu(1)–O(1W)	169.14(11)	Cu(1D)–O(3)–Cu(1E)	91.70(9)
O(3A)–Cu(1)–O(3C)	88.30(9)		

Symmetry transformations: (A) $-x+2$, $y-1/2$, $-z+1/2$; (B) $-x+2,-y+2,-z$; (C) $x,-y+3/2$, $z-1/2$; (D) $-x+2$, $y+1/2$, $-z+1/2$; (E) x, $-y+3/2$, $z+1/2$.

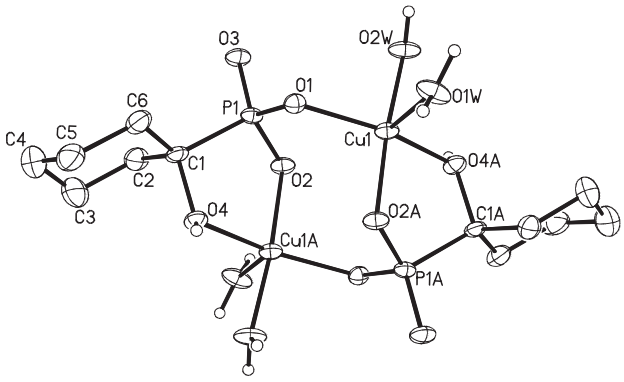

Fig. 1. The binuclear structure of compound **1** with atomic labeling scheme (50% probability). All H atoms except those of water molecules are omitted for clarity.

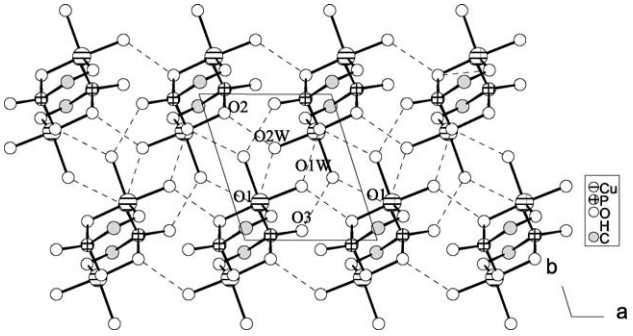

Fig. 2. One layer of compound **1** viewed along *c*-axis. All H and C atoms except C(1) are omitted for clarity.

along the *c*-axis by van der Waals attractions between the organic groups (Fig. 6).

The structure of compound **3** is similar to that of compound **2**, except that the hydroxy oxygen [O(4B)] is replaced by a water molecule [O(1w)] (Fig. 7). Subsequently, the Cu–O bond lengths are in the range 1.912(3)–2.372(2) Å. The Cu(1)…Cu(1) distance over the μ_3-O(3) bridge is 3.124 Å. The Cu(1)–O(3)–Cu(1) bond angle is 91.7°. Figs. 8 and 9 show the inorganic layer of **3** in the *bc* plane and the packing diagram along the [100] direction, respectively. Structure **3** is identical

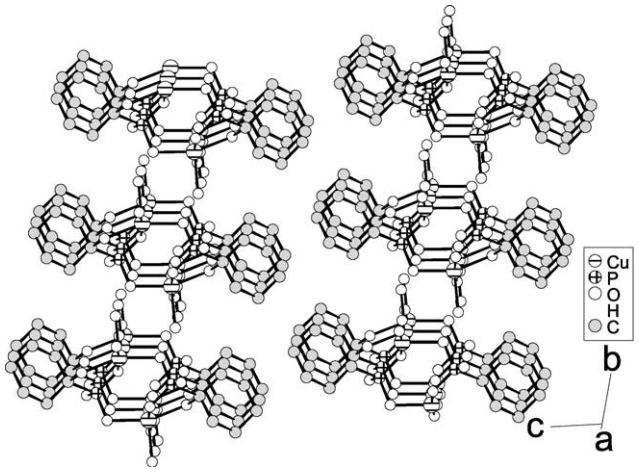

Fig. 3. Packing diagram of compound **1** viewed approximately along *a*-axis. All H atoms are omitted for clarity.

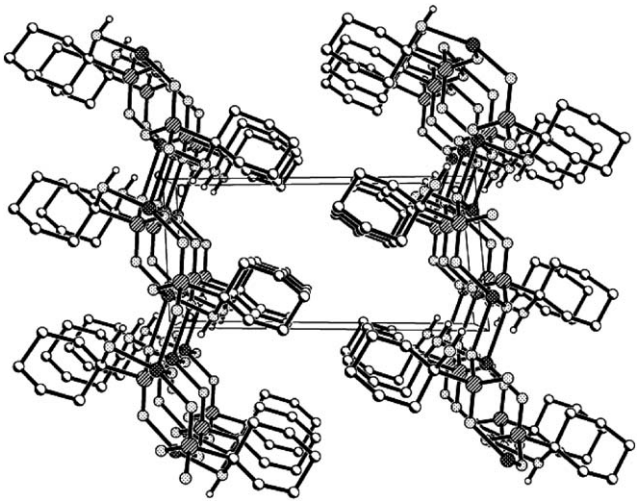

Fig. 6. Packing diagram of compound **2** viewed along *a*-axis. All H atoms are omitted for clarity.

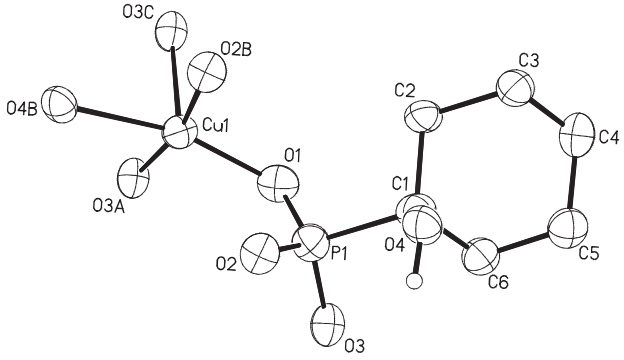

Fig. 4. Building unit of compound **2** with atomic labeling scheme (50% probability). All H atoms except that of the hydroxy group are omitted for clarity.

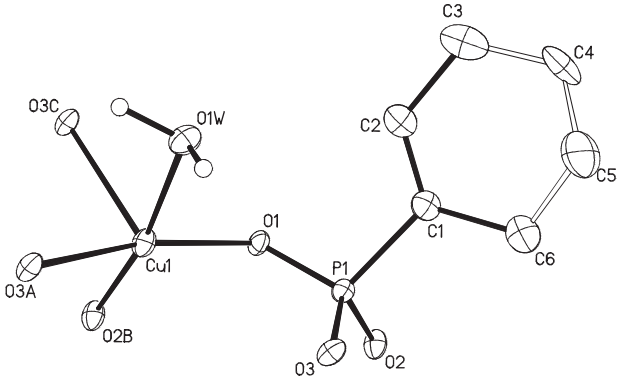

Fig. 7. Building unit of compound **3** with atomic labeling scheme (50% probability). All H atoms except those of water molecules and half of the disordered C atoms [C(4′), C(5′)] atoms are omitted for clarity.

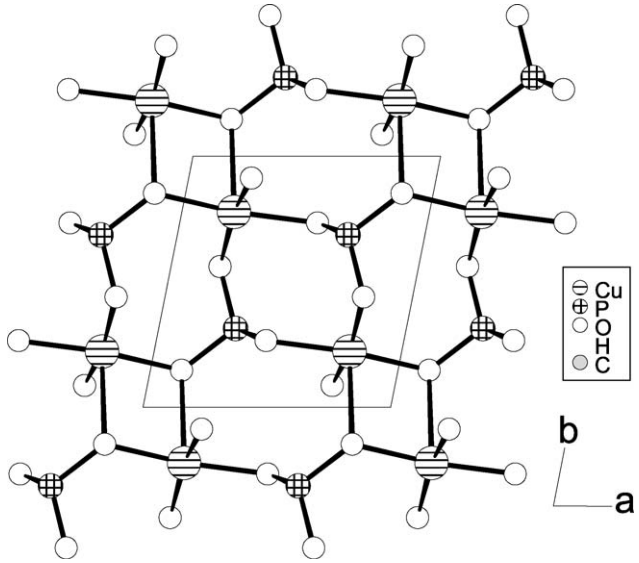

Fig. 5. One inorganic layer of compound **2** viewed along *c*-axis. All H and C atoms are omitted for clarity.

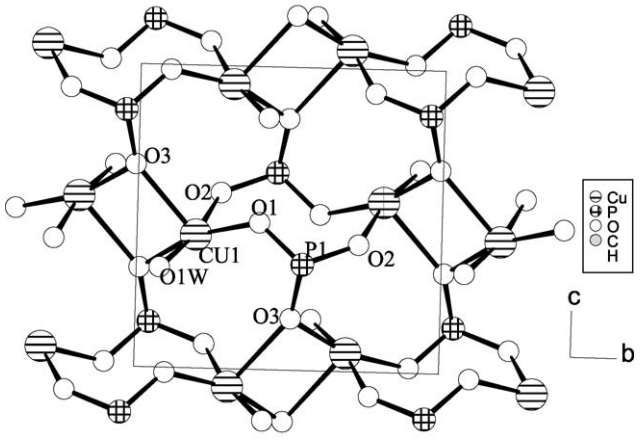

Fig. 8. One inorganic layer of compound **3** viewed along *a*-axis. All H and C atoms are omitted for clarity.

to those of the layer compounds $Cu(RPO_3)(H_2O)$ [16,20].

3.2. Magnetic properties

Fig. 10 shows the χ_M and $\chi_M T$ vs. T plots for **1**. At room temperature, the magnetic moment per Cu is $1.93\,\mu_B$, close to the value ($1.73\,\mu_B$) expected for an isolated spin $S = 1/2$. On cooling, the $\chi_M T$ value increases gradually and reaches a maximum of $0.521\,cm^3\,K\,mol^{-1}$ at 14.5 K, indicating a ferromagnetic coupling between the magnetic centers. The decrease of $\chi_M T$ below 14.5 K could be due to the inter-molecular antiferromagnetic exchanges as well as the zero-field splitting of the ground state. Considering that compound **1** has a dinuclear structure in which the Cu(II) ions are bridged by O–P–O bridges, the susceptibility data were analyzed by Bleaney-Bowers expression based on a Heisenberg Hamiltonian $H = -2JS_1S_2$ [13]:

$$\chi'_M = \frac{Ng^2\beta^2}{kT}\frac{1}{3+\exp(-2J/kT)}(1-\rho) + \frac{Ng^2\beta^2}{4kT}\rho,$$

$$\chi_M = \frac{\chi'_M}{1 - zJ'\chi'_M},$$

where $|2J|$ is the singlet-triplet energy gap and N, g, β and k have their usual meanings. ρ is a variable fraction of paramagnetic impurities. zJ' accounts for the inter-dimer exchanges. A good fit resulted in the solid line in Fig. 10, with the parameters $g = 2.21$, $J = 8.47\,cm^{-1}$, $\rho = 0.0137\%$ and $zJ' = -1.31\,cm^{-1}$.

The χ_M and $\chi_M T$ vs. T plots for **2** and **3** are given in Figs. 11 and 12. The observed magnetic moments per Cu are $1.92\,\mu_B$ for **2** and $1.78\,\mu_B$ for **3** at room temperature. The appearance of a peak at about 5 K in the χ_M vs. T curve is typical for a layered metal phosphonate compound with weak antiferromagnetic interactions. As already described, the inorganic layers of compounds **2** and **3** can be viewed as $\{Cu_2O_2\}$ dimers linked by O–P–O bridges. The magnetic exchange through the oxygen bridge is usually more efficient than that through the O–P–O bridge. Therefore, the magnetic data were also analyzed by the Bleaney-Bowers expression as described above. By neglecting the contribution of paramagnetic impurities, good fits were obtained, shown as solid lines in Figs. 11 and 12, with parameters $g = 2.19$, $J = -3.05\,cm^{-1}$, $zJ' = 0.92\,cm^{-1}$ for **2** and $g = 2.08$, $J = -2.73\,cm^{-1}$, $zJ' = -0.11\,cm^{-1}$ for **3**.

Dominant antiferromagnetic interactions are commonly found in metal phosphonates with layered or pillared layered structures, except compound $Cu_2(H_2O)_2\{O_3PCH_2N(C_2H_4)_2NCH_2PO_3\}$ which shows ferromagnetic interactions [21]. The antiferromagnetic

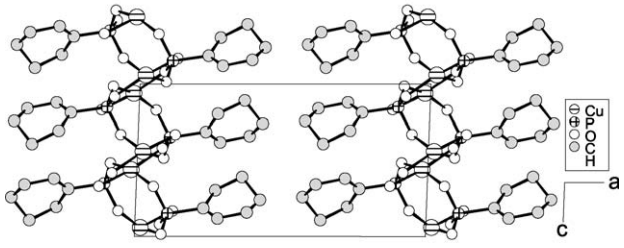

Fig. 9. Packing diagram of compound **3** viewed along *b*-axis. All H atoms and half of the disordered C atoms [C(4′), C(5′)] are omitted for clarity.

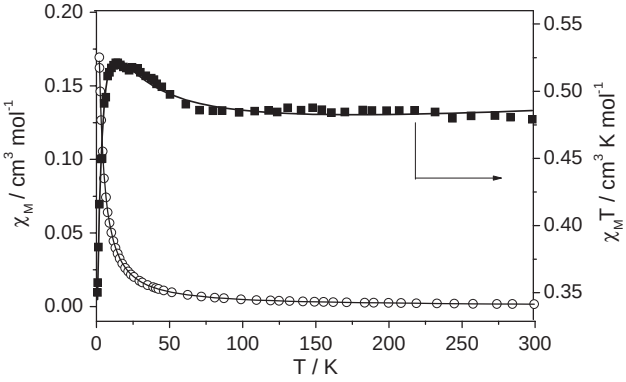

Fig. 10. The χ_M and $\chi_M T$ vs. T plots for **1**.

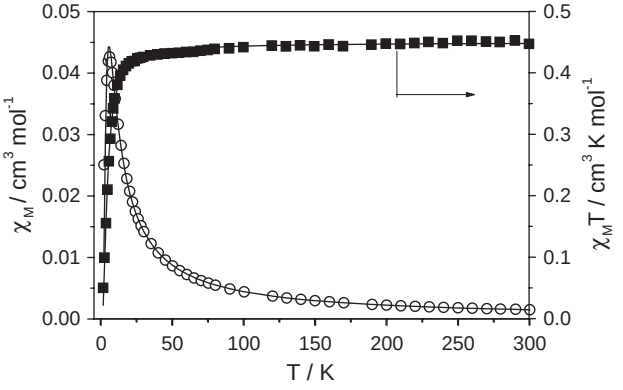

Fig. 11. The χ_M and $\chi_M T$ vs. T plots for **2**.

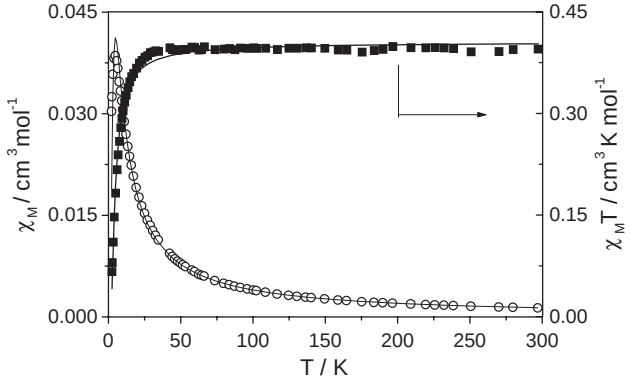

Fig. 12. The χ_M and $\chi_M T$ vs. T plots for **3**.

exchange coupling constants (J) obtained for compounds **2** and **3** are comparable to those for compounds $Cu(RPO_3)(H_2O)$ ($R=CH_3$, C_2H_5, C_6H_5) [17]. The ferromagnetic interaction found in dinuclear compound **1**, however, is unexpected. This ferromagnetic interaction could be caused by the accidental orthogonality of the magnetic orbitals within the dimer. To the best of our knowledge, similar behavior has not been observed in the other copper phosphonates or copper phosphates where the Cu(II) ions are bridged by O–P–O units, except $Cu_2(H_2O)_2\{O_3PCH_2N(C_2H_4)_2NCH_2PO_3\}$ [21].

In summary, three new copper phosphonate compounds, $Cu(C_6H_{10}(OH)PO_3)(H_2O)$ (**1**), $Cu(C_6H_{10}(OH)PO_3)$ (**2**) and $Cu(C_6H_9PO_3)(H_2O)$ (**3**), have been prepared under hydrothermal reaction conditions. Compound **1** has a dinuclear structure, while compounds **2** and **3** exhibit typical layer structures. The magnetic studies reveal that ferromagnetic interactions are propagated in compound **1** and antiferromagnetic interactions in compounds **2** and **3**.

Acknowledgments

The support of the NNSF of China, the Education Ministry of China, the NSF of Jiangsu province (No. BK2002078) and the Analysis Center of Nanjing University are acknowledged. The authors thank Mr. Yong-Jiang Liu for crystal data collection.

References

[1] B. Zhang, A. Clearfield, J. Am. Chem. Soc. 119 (1997) 2751.
[2] G. Alberti, Comprehensive Supramolecular Chemistry, in: J.M. Lehn (Ed.), Vol. 7, Pergamon, Elsevier Science, Ltd., Oxford, UK, 1996.
[3] G. Cao, H. Hong, T.E. Mallouk, Acc. Chem. Res. 25 (1992) 420.
[4] C. Maillet, P. Janvier, M. Pipelier, T. Praveen, Y. Andres, B. Bujoli, Chem. Mater. 13 (2001) 2879.
[5] A. Clearfield, Progress in Inorganic Chemistry, in: K. D. Karlin (Ed.), Vol. 47, Wiley, New York, 1998, p. 371 (and references therein).
[6] K. Barthelet, M. Nogues, D. Riou, G. Ferey, Chem. Mater. 14 (2002) 4910.
[7] E. Burkholder, V. Golub, C.J. O'Connor, J. Zubieta, Inorg. Chem. 42 (2003) 6729.
[8] N. Calin, S.C. Sevov, Inorg. Chem. 42 (2003) 7304.
[9] C. Bellitto, Magnetism: Molecules to Materials II, in: J.S. Miller, M. Drillon (Eds.), Molecule-Based Materials, Wiley-VCH Verlag GmbH & Co. KgaA, New York, 2002, pp. 425–456 (and references therein).
[10] P. Yin, S. Gao, L.-M. Zheng, Z. Wang, X.-Q. Xin, Chem. Commun. (2003) 1076.
[11] L.-M. Zheng, S. Gao, H.H. Song, S. Decurtins, A.J. Jacobson, X.-Q. Xin, Chem. Mater. 14 (2002) 3143.
[12] P. Fay, H.P. Lankelma, J. Am. Chem. Soc. 74 (1952) 4933.
[13] O. Kahn, Molecular Magnetism, VCH Publishers, Inc., New York, 1993.
[14] SAINT, "Program for Data Extraction and Reduction" Siemens Analytical X-ray Instruments, Madison, WI, 1994–1996.
[15] SHELXTL (version 5.0) Reference Manual. Siemens Industrial Automation, Analytial Instrumentation, Madison, WI, 1995.
[16] J. Le Bideau, B. Bujoli, A. Jouanneaux, C. Payen, P. Palvadeau, J. Royxel, Inorg. Chem 32 (1993) 4617.
[17] J. Le Bideau, C. Payen, P. Palvadeau, B. Bujoli, Inorg. Chem. 33 (1994) 4885.
[18] S. Drumel, P. Janvier, M. Bujoli-Doeuff, B. Bujoli, Inorg. Chem. 35 (1996) 5786.
[19] M. Riou-Cavellec, M. Sanselme, N. Guillou, G. Ferey, Inorg. Chem. 40 (2001) 723.
[20] Y. Zhang, A. Clearfield, Inorg. Chem. 31 (1992) 2821.
[21] Y. Wang, S.-S. Bao, W. Xu, J. Chen, S. Gao, L.-M. Zheng, J. Solid State Chem. 177 (2004) 1297.